Macromolecules

pubs.acs.org/Macromolecules Article

Synthesis of Ethylene–Styrene Multiblock Copolymers Possessing High Strength and Toughness Using Binuclear Scandium Catalysts

Qiyuan Wang, Zhen Zhang, Yang Jiang, Shihui Li,* and Dongmei Cui*

Cite This: *Macromolecules* 2025, 58, 2609–2618 Read Online

ACCESS | Metrics & More | Article Recommendations | Supporting Information

ABSTRACT: Synthesizing materials with both high strength and toughness has been a promising but challenging research project. Syndiotactic polystyrene (*s*PS) is known for its high strength while encountering serious brittleness and processing problems. Introducing flexible ethylene units into rigid polystyrene chains can solve these issues, but copolymer regularity and sequence distribution need to be controlled to balance strength and toughness. Herein, we report the copolymerization of styrene and ethylene using alkyl-bridged fluorenyl binuclear scandium catalysts. The resulting copolymers show superior tensile strength (60.0 MPa) and impact resistance (119.6 kJ m^{-2}), surpassing *s*PS and high-density polyethylene (HDPE), respectively. These properties are mainly attributed to their unique chain structures composed of long syndiotactic polystyrene and long polyethylene multiblocks, forming an interpenetrating network without phase separation. The PE sequence lengths were measured by successive self-annealing procedures. The density functional theory simulation revealed the mechanisms. The binuclear active species of homo *s*PS-attached Sc^{3+} species ($\mathbf{Cat_{Sc2\text{-}nSt}}$) prefer styrene insertion due to low insertion energy and thermostable intermediate. Homo PE-attached Sc^{3+} ions ($\mathbf{Cat_{Sc2\text{-}nE}}$) favor ethylene insertion, where the agoistic interaction of H---Sc^{3+} prevents styrene insertion. The hetero *s*PS and PE-attached Sc^{3+} ions ($\mathbf{Cat_{Sc2\text{-}nESt}}$) provide the opportunity to form *s*PS–PE joints in the copolymer chain.

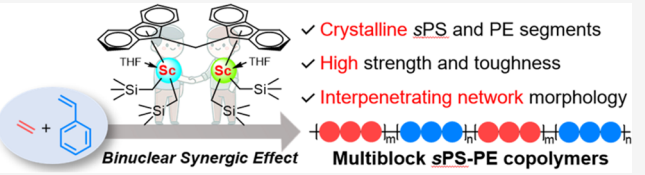

INTRODUCTION

To synthesize a material possessing properties of high strength and toughness simultaneously has been a research challenge. Syndiotactic polystyrene (*s*PS), an engineering plastic renowned for its high melting point, crystallinity, mechanical strength, and elastic modulus,[1−3] has abstracted immediate attention from both academia and industrial worlds since it was first discovered by Ishihara and colleagues in 1986.[4,5] Significant achievements have been made with respect of polymerization activity and stereoselectivity by designing new early transition metal or rare-earth metal-based complexes bearing cyclopentadienyl (Cp) and its derivative ligands and the constrain-geometry-configuration (CGC) ligands.[6−15] However, the brittleness and high processing temperature of *s*PS have prohibited its widespread applications. To overcome these issues, numerous strategies have been proposed such as blending *s*PS with glass fiber and carbon fiber or via postpolymerization modification. The copolymerization of styrene (St) with functionalized styrene derivatives or other monomers is a direct and promising strategy,[16,17] since it provides materials with tailored properties by adjusting the composition and sequence of the main chains.[18] Of these, copolymerization with ethylene (E) has emerged in a particularly intriguing manner because introducing flexible polyethylene (PE) segments into the rigid *s*PS backbone is anticipated to enhance its toughness and reduce the processing temperature effectively. The copolymerization of St and E with Ziegler–Natta catalysts is unsuccessful by yielding a mixture of homopolymers and a copolymer with a very low St content.[19−21] The half-sandwich titanium catalysts represented by $Cp'TiX_3$ (X = Cl, OMe, etc.) exhibit excellent activity toward both E and St but show low activities in copolymerization and afford a mixture of PE, *s*PS, and an atactic copolymer.[10,22−25] Bearing anionic ancillary donor catalysts composed of $Cp'TiX_2Y$ (Y = anionic ligand) show highly increased activity for the copolymerization and afford pure copolymers albeit lacking the melting point associated with *s*PS segments.[9,26,27] Similarly, CGC-Ti catalysts can produce the random copolymer although without *s*PS characteristics.[28−30] Binuclear CGC-Ti catalysts display higher St insertion ratios owing to the binuclear synergistic effect while affording stereoirregular copolymers without a T_m.[31] The problems of Ti-based catalysts generating a mixture of homopolymers or a copolymer without an *s*PS sequence are mainly ascribed to the facile valence change of the Ti active species during the polymerization process. Ti(IV) probably produces PE and atactic PS-E copolymer,[32,33] while it is reduced (partly) to Ti(III), the true active species for giving

Received: January 21, 2025
Revised: February 10, 2025
Accepted: February 13, 2025
Published: February 17, 2025

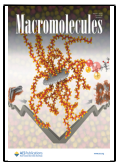

https://doi.org/10.1021/acs.macromol.5c00169
Macromolecules 2025, 58, 2609–2618

Scheme 1. Structure of Mono- and Binuclear Scandium Catalysts Sc_1, C2−Sc_2, and C1−Sc_2

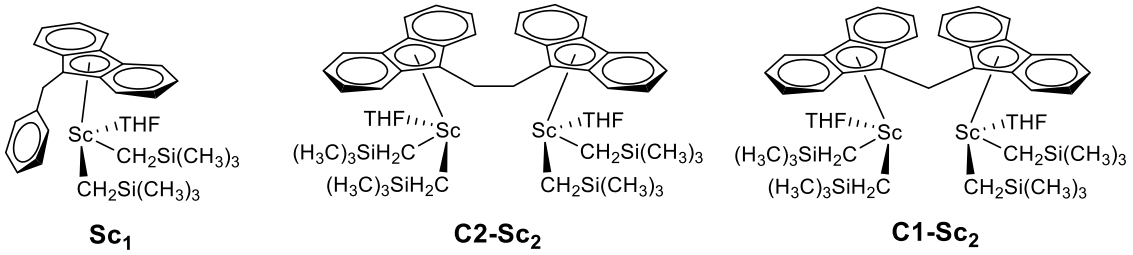

Table 1. Homo- and Copolymerization of St with E Using Mono- and Binuclear Scandium Catalysts Sc_1, C2−Sc_2, and C1−Sc_2[a]

run	cat.	[St]:[Sc]:[Al] (mol:mol:mol)	time (min)	temp. (°C)	conv. (%)	yield (g)	act.[c] (10^6)	M_n[d] (10^4)	M_w/M_n[c]	f_{St}[e] (%)	T_m[f] (°C)	ΔH[f] (J g^{-1})
1[b]	Sc_1	500:1:5	2	25	90	0.94	1.36	37.4	1.89	100	268.4	19.3
2[b]	C2−Sc_2	500:1:5	2	25	15	0.16	0.24	44.3	2.05	100	268.6	15.0
3[b]	C1−Sc_2	500:1:5	5	25	17	0.18	0.11	78.2	2.02	100	268.7	20.9
4	Sc_1	2000:1:10	5	40	98	5.21	3.13	12.8 (**P1**)	2.20	49.1	207.4	4.6
5	C2−Sc_2	2000:1:10	10	40	25	1.85	0.55	38.0 (**P2**)	1.40[g]	26.4	128.9, 222.5	50.2, 3.5
6	C1−Sc_2	2000:1:10	10	40	22	1.73	0.52	47.7 (**P3**)	1.29[g]	23.8	129.0	36.6
7	C1−Sc_2	2000:1:10	10	60	47	3.29	0.99	43.2	1.32[g]	27.9	127.7, 218.0	36.1, 2.6
8	C1−Sc_2	2000:1:10	10	80	50	3.22	0.97	31.0	1.64[gh]	32.6	125.4, 231.4	28.6, 5.9
9	C1−Sc_2	4000:1:10	10	60	38	3.98	1.19	47.6 (**P4**)	1.80	50.6	126.5, 238.1	15.9, 5.5
10	**Sc1**	8000:1:10	1	60	93	15.69	47.08	43.3 (**P5**)	2.65	93.9	248.6	15.5
11	C2−Sc_2	8000:1:10	8	60	47	8.64	3.24	51.8 (**P6**)	2.08	72.0	123.1, 255.2	2.3, 11.9
12	C1−Sc_2	8000:1:10	10	60	25	4.77	1.43	80.1 (**P7**)	2.42	67.9	125.8, 243.6	2.6, 6.0

[a]General conditions: Sc_1, 20 μmol; C2−Sc_2 and C1−Sc_2, 10 μmol; $[Ph_3C][B(C_6F_5)_4]$, 20 μmol; chlorobenzene, 40 mL; ethylene pressure = 4 bar. [b]Homopolymerization of styrene. [c]Given in g mol_{Sc}^{-1} h^{-1}. [d]Determined by GPC in in 1,2,4-trichlorobenzene at 150 °C against polystyrene standard. [e]Determined by ^1H NMR spectrum in $C_6D_4Cl_2$ at 110 °C ($f_{St} = 4A_{ar}/(5A_{al}+A_{ar}) \times 100\%$, where A_{ar} = area of aromatic protons and A_{al} = area of aliphatic protons). [f]Determined by DSC. [g]GPC traces of the copolymers exhibiting up and down peaks. [h]Figure S19 of DOSY spectrum analysis proves the sample is a pure copolymer not a mixture.

*s*PS,[8] by excessive methyl aluminum oxide (MAO)[34] or styrene in the presence of MAO[32] or borate.[35] Currently, only a few Ti catalysts provide a syndiotactic copolymer with one T_m from *s*PS sequences.[36] The landmark work is attributed to the half-sandwich lanthanide scandium catalytic system, Cp'Sc-$(CH_2SiMe_3)_2(THF)$, which achieves highly efficient copolymerization to give E−St copolymers with syndiotacticity and variable St contents but one T_m arising from *s*PS sequences.[12] The subsequent developed half-sandwich scandium catalysts bearing the fluorenyl or hydrogenated fluorenyl ligands exhibit similar characteristic catalysis with respect to the activity and the copolymer structure.[37−39] The allyl *ansa*-neodymocene (Flu-CMe_2-Cp)Nd(η^3-C_3H_5)(THF) catalyst produces E−St copolymers composed of long *s*PS sequences separated by discrete E units to give a T_m varying within 205−241 °C depending on the St content.[13] Obviously, Lewis acidic scandium metal-based catalysts show the intrinsic priority toward St polymerization as compared to E, prohibiting the formation of long PE blocks in the copolymerization procedure. For scandium catalysts bearing the electron-withdrawing pyridinyl fluorenyl or the thiophene-fused cyclopentadienyl ligands, the more Lewis acidic metal center prefers E insertion by giving copolymers composed of long PE sequences (a T_m around 125 °C) separated by discrete St units.[40] Therefore, St/E copolymers maintaining the characteristics of both PE and *s*PS, especially the mostly concerned trade-off between strength and toughness, have still not been achieved, nor the properties have been known.

Herein, we report the copolymerization of St and E by using binuclear scandium catalysts attached to the alkyl-bridged fluorenyl ligands (highly active toward E copolymerization with polar monomers[41,42]) to afford multiblock polymers containing both long *s*PS and PE sequences and two T_m values. Comprehensive characterizations of the chain structure and phase morphology were conducted, which reveal, for the first time, the structural characteristics of high strength and tough E−St copolymer. The involved mechanisms were elucidated by DFT simulations.

RESULTS AND DISCUSSION

The half-sandwich mononuclear scandium catalyst Sc_1 and the binuclear scandium catalysts C2−Sc_2 and C1−Sc_2 were prepared following the reported procedures (Scheme 1).[41] The mononuclear Sc_1 and the flexible binuclear C1−Sc_2 were highly active toward E homopolymerization upon activation with organo borate $[Ph_3C][B(C_6F_5)_4]$ and aluminum alkyls. Sc_1 produced medium-molecular-weight PEs, probably due to β-H elimination caused by the sterically less bulky coordination sphere. The binuclear C1−Sc_2 exhibited similar activity to Sc_1 but afforded ultrahigh-molecular-weight PEs, since the synergic effect of the rigid and crowded binuclear structure inhibited β-H chain transfer.[41] Then, St homopolymerization

https://doi.org/10.1021/acs.macromol.5c00169
Macromolecules 2025, 58, 2609−2618

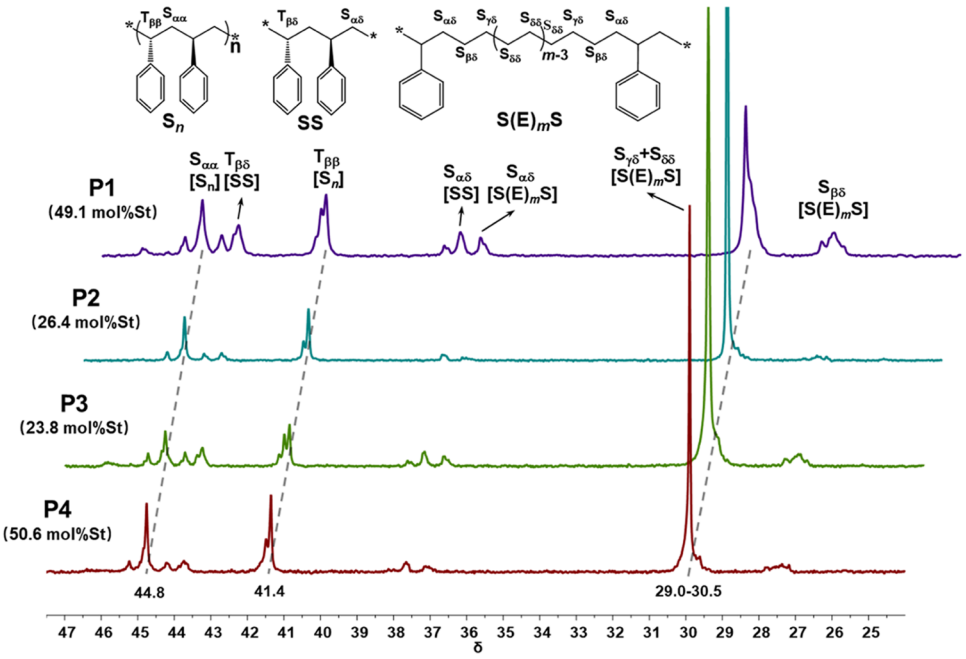

Figure 1. ^{13}C NMR (100 Hz, 110 °C, $C_6D_4Cl_2$) spectra of PS-*co*-PE: Table 1, run 4 (**P1**), run 5 (**P2**), run 6 (**P3**), and run 9 (**P4**).

was evaluated. The mononuclear **Sc$_1$** exhibited the highest activity of 1.36 × 10^6 g mol_{Sc}^{-1} h^{-1}, which is 5 times and 10 times higher than those of the binuclear scandium catalysts **C2−Sc$_2$** (0.24 × 10^6 g mol_{Sc}^{-1} h^{-1}) and **C1−Sc$_2$** (0.11 × 10^6 g mol_{Sc}^{-1} h^{-1}), respectively. Obviously, the more opening coordination sphere is, the higher the activity is, fitting well with the trend of buried volume **Sc$_1$** < **C2−Sc$_2$** < **C1−Sc$_2$** (16.1, 18.6, and 19.6%; Figure S1), since the less steric metal center facilitates coordination and insertion of the large St monomer. On the contrary, the highest-molecular-weight PS was isolated from the most sterically bulky system **C1−Sc$_2$**, since *β*-H-elimination, chain-transfer reactions, etc. were completely prohibited (78.2 × 10^4 g mol^{-1} vs 44.3 × 10^4 g mol^{-1} and 37.4 × 10^4 g mol^{-1}) (Table 1, runs 1−3), in agreement with E polymerization results.[41] Despite the catalyst precursors, all of the isolated PS are syndiotactic (*s*PS), as evidenced by a single sharp resonance at 145.5 ppm in the ^{13}C NMR spectrum (Figure S32) and a high melting point of around 268 °C.

The dual catalytic activities of these systems toward both E and St polymerizations encouraged us to investigate their performances for E and St copolymerization. When subjected to the St-to-Sc feed ratio of 2000:1 under a 4 bar of E atmosphere and a temperature of 40 °C, the activity followed the trend of **Sc$_1$** > **C2−Sc$_2$** > **C1−Sc$_2$** (3.13 × 10^6 g mol_{Sc}^{-1} h^{-1} vs 0.55 × 10^6 g mol_{Sc}^{-1} h^{-1} vs 0.52 × 10^6 g mol_{Sc}^{-1} h^{-1}). Meanwhile, the molecular weight of the resultant copolymer **P1** isolated from **Sc$_1$** (12.8 × 10^4 g mol^{-1}) is smaller than **P2** from **C2−Sc$_2$** (38.0 × 10^4 g mol^{-1}) and **P3** from **C1−Sc$_2$** (47.7 × 10^4 g mol^{-1}) (Table 1, runs 4−6). Obviously, the performances of these catalytic systems for copolymerization remained like those of homopolymerizations with respect to activity and the molecular weight of the resultant product. Fixing at the same conditions but carrying out the copolymerization at a higher temperature of 60 °C with the catalyst **C1−Sc$_2$**, both the activity and St conversion were almost doubled, and St incorporation also increased due to the mobility of polymer chains. Meanwhile the molecular weight dropped obviously due to the increased chain-transfer reaction under a high temperature. Further elevating the reaction temperature to 80 °C resulted in slightly improved St conversion and incorporation as well as activity, which was accompanied by a dramatic decrease of the molecular weight due to the serious chain transfer (Table 1, runs 7 and 8). Noteworthy was that the GPC curve of the copolymer with a lower St content (Table 1, runs 5−8) shows up and down signals, which are attributed to different styrene and ethylene contents in different molecular weight fractions within one copolymer rather than a mixture of PE and *s*PS homopolymers. The higher-molecular-weight fraction containing more styrene units gives an up peak, while the lower-molecular-weight fraction containing more ethylene units gives a down peak. This is confirmed by the uniform dispersity of the copolymer in the DOSY spectrum (Figure S19). Compared to polymerization temperature, varying St loading brought about more significant changes not only in the activity but also in the composition of the product. Increasing the St-to-Sc ratio stepwise from 2000:1 to 8000:1, in the case of using **Sc$_1$** as the catalyst precursor, the activity increased 15 times to 4.7 × 10^7 g mol_{Sc}^{-1} h^{-1} accompanied by the overwhelming St incorporation in the product (93.9 vs 49.1 mol %) under a similar high St conversion (98 vs 93%) (Table 1, runs 4 and 10). When **C2−Sc$_2$** and **C1−Sc$_2$** were employed, both the activity and St content increased significantly as compared to those at low St-to-Sc ratios, but the variations were not as obvious as those of the **Sc$_1$** system (Table 1, runs 5, 6, 11, 12), indicating that high St loading facilitated the copolymerization by accelerating St incorporation while E insertion was still active. Without surprise, molecular weights (up to 80.1 × 10^4 g mol^{-1}) of copolymers isolated from **C2−Sc$_2$** and **C1−Sc$_2$** catalytic systems are much higher than that from the **Sc$_1$** system despite the St-to-Sc ratio and polymerization temperature, since the sterically bulky active metal centers reduced *β*-H-elimination and chain-transfer reactions. Changing polymerization conditions caused apparent variations in the activity and the molecular weight of the resultant copolymer, which

https://doi.org/10.1021/acs.macromol.5c00169
Macromolecules 2025, 58, 2609−2618

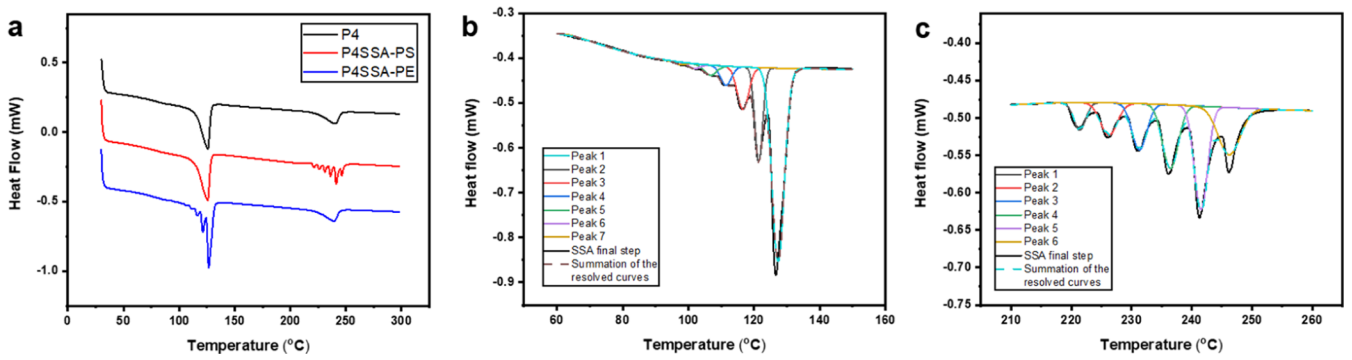

Figure 2. (a) DSC curves of E−St copolymer **P4** (red and blue curves were determined after treating the samples by a successive self-nucleation and annealing procedure). The heat flow results of the final melting step in the successive self-nucleation and annealing procedure: (b) PE part and (c) *s*PS part.

deeply influenced the composition and sequence distribution and, subsequently, the morphology and physical and mechanical properties. Thus, further characterization of the primary chain structures of the resultant copolymers was carried out. The ^{13}C NMR spectrum of copolymer **P1** isolated from $\mathbf{Sc_1}$ gives strong resonances at 44.8 and 41.4 ppm attributed to the short consecutive *s*PS sequence of SS (PE-St-St-PE) and long consecutive *s*PS sequence of S_n (PE-$(St)_n$-PE) (Figure 1), respectively, and the peak at 29.0−30.5 ppm assigned to the long PE sequence of $S(E)_mS$. Although the St content in **P1** is as high as 49.1 mol %, the characteristic peak at 46.5 ppm representing discrete St units is clearly observed. On the contrary, for copolymers **P2** and **P3** bearing a much lower St unit content (26.4 mol % vs 23.8%) isolated from $\mathbf{C2-Sc_2}$ and $\mathbf{C1-Sc_2}$, the relative integrated intensities of both S_n and long PE resonances become stronger as compared to those in **P1**, while resonances for the discrete St units are rather weak or nearly invisible. The DSC trace of **P1** (Figure S23) shows one melting point (T_m) around 207.7 °C with ΔH of 4.6 J g^{-1} from *s*PS sequences, which is lower than those of the *s*PS homopolymer (268 °C, ΔH = 19.3 J g^{-1}).[12] In addition, no T_m corresponding to PE is present, although the E content is even slightly more than that of St (50.9 vs 49.1%). This suggests that **P1** possesses a multiblock chain structure, where *s*PS sequences are longer enough to crystallize while PE sequences are too short (<25 repeated units) to crystallize.[43,44] For **P5** isolated from the same catalyst system ($\mathbf{Sc_1}$) under a high St loading, the presence of a small amount of PE units (6.1%) interrupts the continuity of *s*PS chains, resulting in a decreased melting point T_m of 248.6 °C with an entropy of 15.5 J g^{-1} (Figure S29), which are still lower than those of *s*PS but higher than those of **P1**. It is reasonable that no T_m is ascribed to PE sequences observed in **P5**. Obviously, for the $\mathbf{Sc_1}$ system, it is rather difficult to form long PE sequences in the obtained copolymers due to too rapid St propagation, although the E fraction in the copolymer can be as high as 50.9%. For catalytic systems $\mathbf{C2-Sc_2}$ and $\mathbf{C1-Sc_2}$, the isolated copolymers **P2** and **P3** bearing much lower St contents (26.4 and 23.8 mol %) as compared to **P1** and **P5** still exhibit the characteristic peaks of S_n despite giving a weak or none crystalline peak (DSC traces of Figures S26 and S27). Noteworthy was that both **P2** and **P3** contain long enough PE sequences to crystallize by providing a T_m at 128.9 and 129 °C, respectively, with a high ΔH value (50.2 J g^{-1} and 36.6 J g^{-1}). These results approached our original target of finding catalytic systems like $\mathbf{C2-Sc_2}$ and $\mathbf{C1-Sc_2}$ to carry out the copolymerization under a high St loading to ensure propagating long *s*PS sequences while PE sequences are also long enough to crystallize to maintain *s*PS bulk properties. Finally, **P6** and **P7** bearing high St contents (72 and 67.9%) were synthesized, which exhibit two T_ms at 255.2 and 123.2 °C for **P6** and at 243.6 and 125.8 °C for **P7**, correlating with long *s*PS and long PE sequences.

To further investigate the length and distribution of PE and *s*PS blocks in the copolymer, successive self-nucleation and annealing (SSA) treatment was conducted on **P4** containing 50.6 mol % styrene units. The SSA-DSC curves of **P4** reveal several distinct endothermic peaks within the temperature ranges of 97−127 °C for PE segments and 221−246 °C for *s*PS segments (Figure 2). According to the fitting results of the peaks (Table S2), PE segments with the highest melting point (127 °C) occupy 59.4% of the population, while those with the lowest melting point (97 °C) occupy only 0.6%, indicating a significantly homogeneous distribution. Each melting peak correlates to PE segments with similar E sequence lengths (ESL) that are estimated using eq 1 (e = natural constant, T = melting temperature of PE sequence).[45,46] The length of the crystalline PE segment in **P4** ranges from 25 to 97 E units, with long sequences occupying a large population. In contrast, the distribution of *s*PS segments is more broad. The segments correlating to the melting point of 242 °C exhibit the highest proportion (27.7%), while the segments with the lowest melting point (221 °C) still account for 6.5%. Unfortunately, due to the lack of reports about the relationship between *s*PS segment length and melting point, the length of the *s*PS segments in the copolymer could not be calculated. Nonetheless, the SSA results indicate that the length of the *s*PS segment in the copolymers is variable but long enough to crystallize, whereas the PE segments are predominantly long. This proved again the importance of the catalytic system for this copolymerization, and the sequence length distribution such as **P4** from $\mathbf{C1-Sc_2}$ and **P1** from $\mathbf{Sc_1}$ has similar composition but different sequence distribution and properties.

$$\mathrm{ESL} = \frac{1}{e^{142.2/T-0.3451} - 1} \tag{1}$$

To establish the relationship between the primary structure and mechanical properties, various copolymers with different St contents were prepared through scaled-up experiments (Table S1), which evaluated the most important tensile strength and impact resistance and provided a comparison

https://doi.org/10.1021/acs.macromol.5c00169
Macromolecules 2025, 58, 2609−2618

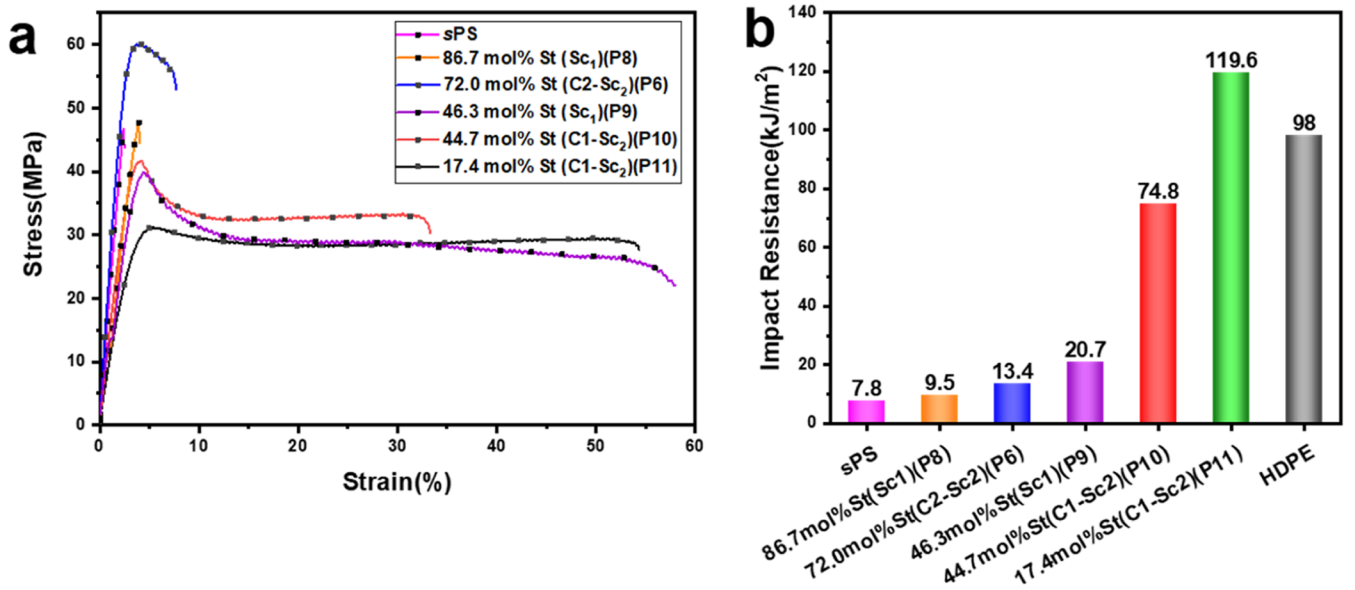

Figure 3. (a) Stress−strain curves for E−St copolymers and commercial *s*PS. (b) Impact resistance of E−St copolymers, commercial *s*PS and HDPE.

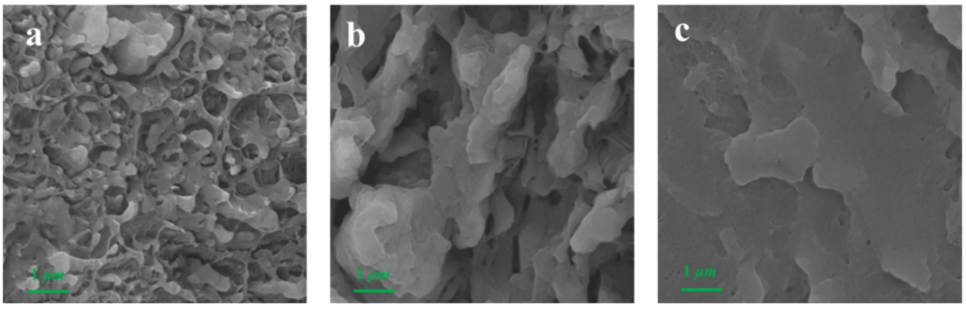

Figure 4. SEM pictures of E−St copolymers prepared with **C1**−$\mathbf{Sc_2}$/**C2**−$\mathbf{Sc_2}$ (Table S1): (a) 17.4 mol % St content (**P11**), (b) 44.7 mol % St content (**P10**), and (c) 72.0 mol % St content (**P6**).

between the commercially accessible *s*PS and high-density PE (HDPE) (Figure 3). The commercial *s*PS (pink line) has a high strength of 47 MPa but is very brittle, with a low elongation at break of 2.3% and a low impact resistance of 7.8 kJ m^{-2}. Copolymer **P8** prepared from $\mathbf{Sc_1}$ containing 86.7 mol % St content by incorporating a small number of E units (orange line) shows a slight increase in the elongation at break (3%) but a significant drop in T_m (240.5 vs 268 °C for *s*PS), probably because the short PE sequences destroy the crystallinity of *s*PS. Strikingly, **P6** produced by **C2**−$\mathbf{Sc_2}$ with a further reduced St content of 72 mol % (blue line) exhibits an exceptionally high tensile strength of 60.0 MPa and doubled elongation at break (7.7%) and impact resistance (13.4 kJ m^{-2}) as compared to **P8**, significantly surpassing those of commercial *s*PS. These improvements can be attributed to the incorporation of flexible long PE segments evidenced by the presence of T_m (123.1 °C), which effectively hindered the cracking development and rapid propagation during stress. Copolymer **P9** synthesized by $\mathbf{Sc_1}$ with a medium St content of 46.3 mol % (purple line) behaves as a tough material by reaching a yield point of 39.9 MPa and a much-modified break elongation of 58% as well as a high impact resistance of 20.7 kJ m^{-2}, which is contributed to the presence of consecutive PE sequences albeit with an obvious drop in strength (28.5 MPa) as usually found in tough materials. Noted that copolymer **P10** with a similar St content (44.7 mol %) to **P9** but prepared from **C1**−$\mathbf{Sc_2}$ (red line) displays a similar yielding point (41.8 MPa), a slightly increased strength (32 MPa), and a slightly decreased final break elongation of 35.0%, surprisingly, to give a distinguished impact resistance up to 74.8 kJ m^{-2}. The big difference in the impact resistances of **P9** and **P10** was due to different sequence distributions. For **P9** prepared by $\mathbf{Sc_1}$ with an opening coordination sphere to propagate St rapidly, PE sequences are not long enough to toughen *s*PS, as proved by only one T_m corresponding to *s*PS. For **P10**, there are two T_ms corresponding to both long PE and *s*PS sequences, respectively. When **P10** is subjected to high-intensity and short-duration impacts, *s*PS molecular chain movement becomes highly localized, while relatively flexible, long, and uniformly distributed PE segments behave as modifiers to absorb energy and enhance toughness. On the other hand, incorporating a small amount of *s*PS segments into PE can increase both its tensile strength and impact resistance. For instance, copolymer **P11** produced by **C1**−$\mathbf{Sc_2}$ (black line) exhibited a notable strength of 30.0 MPa, an elongation at break of 54.3%, and a high impact resistance of 119.6 kJ m^{-2}, where long PE sequences (evidenced by the high ΔH value 74.0 J g^{-1}) are separated by the small amount of short *s*PS sequences (17.4 mol %). As such, by varying the sequence distribution, the E-*s*PS copolymers can be high-strength

https://doi.org/10.1021/acs.macromol.5c00169
Macromolecules 2025, 58, 2609−2618

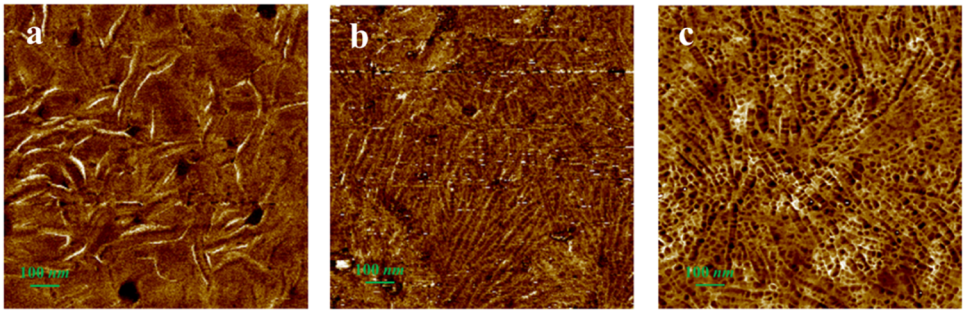

Figure 5. AFM pictures of E−St copolymers prepared with **C1**−Sc_2/**C2**−Sc_2 (Table S1): (a) 17.4 mol % St content (**P11**), (b) 44.7 mol % St content (**P10**), and (c) 72.0 mol % St content (**P6**).

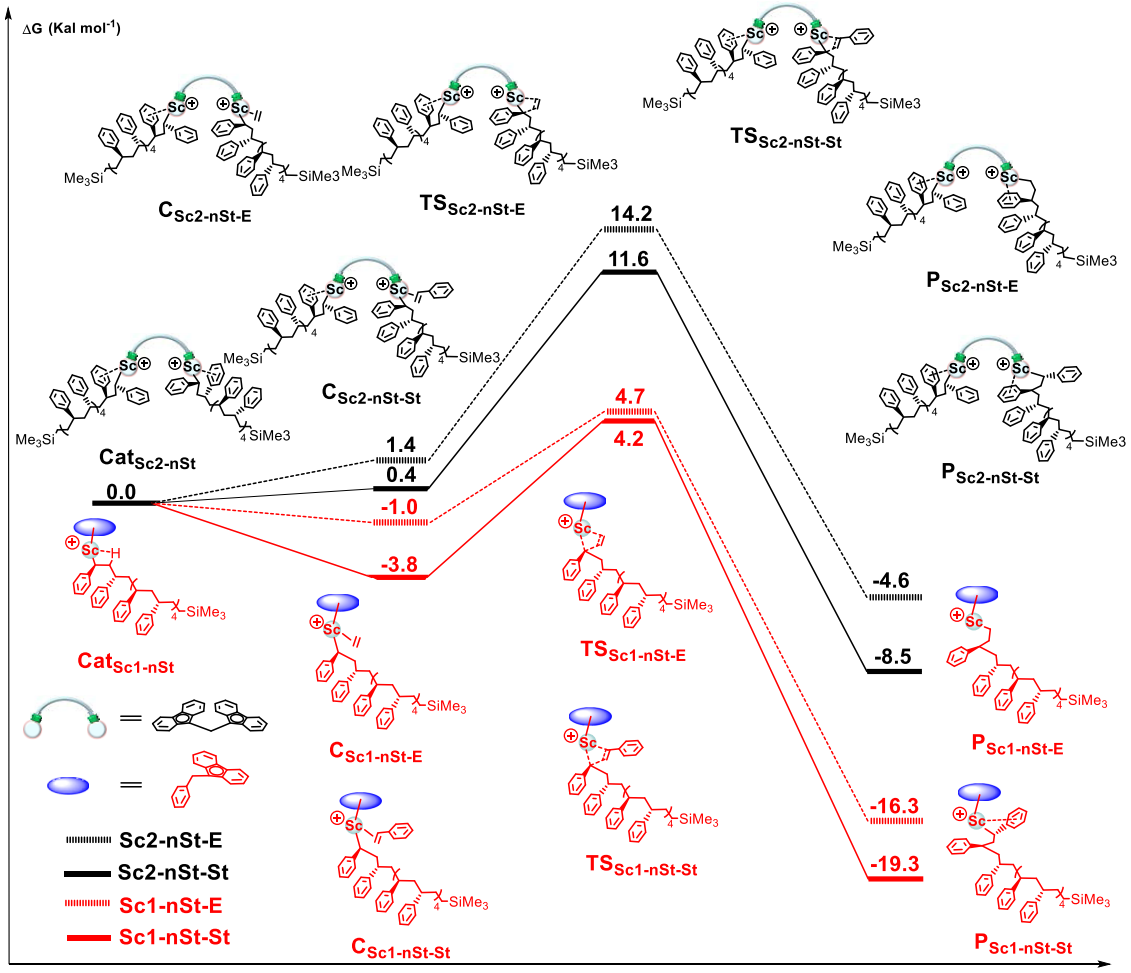

Figure 6. Energy profiles from the DFT simulation for chain growth of styrene−ethylene copolymerization catalyzed by *s*PS-ended active species $Cat_{Sc1\text{-}nSt}$ and $Cat_{Sc2\text{-}nSt}$.

materials with tough properties surpassing those of *s*PS or HDPE.

The performances of polymers are closely correlated to their microstructures, where multiblock copolymers often exhibit characteristics of large-scale uniformity and fine-scale separation. Scanning electron microscopy (SEM) was employed to investigate the cross sections of the copolymers. It was observed that copolymers **P6**, **P10**, and **P11** from **C1**−Sc_2 do not exhibit obvious phase separation despite St contents (72.0% vs 44.7% vs 17.4%) (Figure 4). Atomic force microscopy (AFM) was used to characterize phase separation on the surfaces of polymer films. When the styrene content is low, the rigid syndiotactic *s*PS phase appears as island-like structures uniformly distributed within the PE phase (Figure 5a). For moderate St content, the phase diagram shows the presence of filamentous *s*PS phases that divide PE into bands (Figure 5b). At very high St content, the two phases are fully integrated, forming a bicontinuous structure (Figure 5c). Wide-angle X-ray diffraction (WAXD) analysis of the copolymers reveals the coexistence of crystalline regions corresponding to both *s*PS and PE, indicating the presence of long-chain structures in both segments (Figure S3). This characterization further supports the notion that the

https://doi.org/10.1021/acs.macromol.5c00169
Macromolecules 2025, 58, 2609−2618

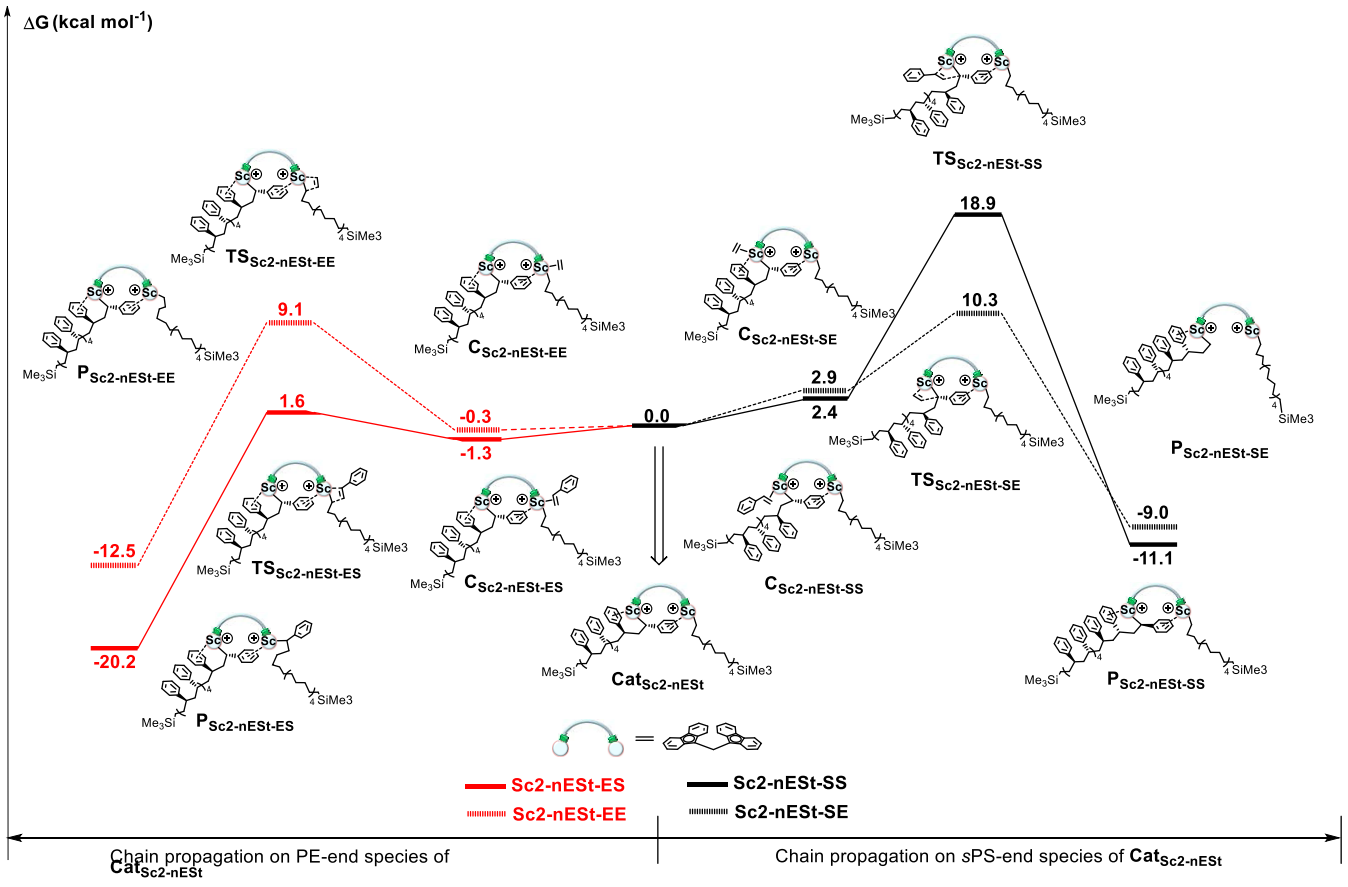

Figure 7. Energy profiles of the DFT simulation for chain growth of the styrene−ethylene copolymerization catalyzed by active species $\mathbf{Cat_{Sc2\text{-}nESt}}$.

copolymer consists of *s*PS and PE segments with extended chain lengths.

The mechanisms of the copolymerization process mediated by mononuclear **Sc1** and binuclear **C1**−$\mathbf{Sc_2}$ were simulated by density functional theory (DFT) calculations. In the initiation stage, both **Sc1** and **C1**−$\mathbf{Sc_2}$ preferentially undergo St coordination−insertion, since the strong coordination ability of St and the back-coordinating of the penultimate phenyl ring help to stabilize the Sc^{3+} active center (Figure S4). Therefore, we proposed a scenario in which long *s*PS sequences were first generated in **C1**−$\mathbf{Sc_2}$, as depicted in Figure 6. Due to the huge steric hindrance, the two *s*PS segments adopt backward ($\mathbf{Cat_{Sc2\text{-}nSt}}$, 0 kcal mol^{-1}) rather than parallel arrangement ($\mathbf{Cat_{isoSc2\text{-}nSt}}$, 1.0 kcal mol^{-1}) (Figure S5), thus, *s*PS-ended $\mathbf{Cat_{Sc2\text{-}nSt}}$ was selected as the active species. $\mathbf{Cat_{Sc2\text{-}nSt}}$ adopting the next St monomer requires to overcome an energy barrier of 11.6 kcal mol^{-1} through the transition state of $\mathbf{TS_{sc2\text{-}nSt\text{-}St}}$, which is 2.6 kcal mol^{-1} lower than propagating E via $\mathbf{TS_{sc2\text{-}nSt\text{-}E}}$. Moreover, the resultant intermediate $\mathbf{P_{Sc2\text{-}nSt\text{-}St}}$ is more thermodynamically stable (−8.5 kcal mol^{-1}) than the E propagation intermediate $\mathbf{P_{Sc2\text{-}nSt\text{-}E}}$ (−4.6 kcal mol^{-1}). Obviously, the active species $\mathbf{Cat_{Sc2\text{-}nSt}}$ is favored to incorporate St, leading to the generation of longer *s*PS segments. A similar situation was observed when the active species is *s*PS-ended mononuclear **Sc1**, which kinetically prefers St chelating to E (−3.8 kcal mol^{-1} vs −1.0 kcal mol^{-1}) and affords thermodynamically more stable intermediate $\mathbf{P_{Sc1\text{-}nSt\text{-}St}}$ with 3.0 kcal mol^{-1} advantage than $\mathbf{P_{Sc1\text{-}nSt\text{-}E}}$. Overall, the activation energy of propagating St for the catalytic system **Sc1** is rather lower than that for the binuclear system **C1**−$\mathbf{Sc_2}$, in agreement with the experiment results that the former is more active than the latter due to the less steric coordination environment.

When long PE-ended **C1**−$\mathbf{Sc_2}$ is the active species, $\mathbf{Cat_{Sc2\text{-}nE}}$ (Figure S6, black), the two PE chains can arrange in parallel mode, and multiple H-agoistic chelation between the hydrogen atoms on the PE chains and the Sc^{3+} ions are observed,[41] demonstrating the significant synergistic effect. The coordination of smaller E monomer to $\mathbf{C_{Sc2\text{-}nE\text{-}E}}$ is 5.0 kcal mol^{-1} advantage accompanied by partly dissociating H-agoistic chelation from one Sc^{3+} ion and the subsequent E insertion is still easy (5.5 kcal mol^{-1}). On the contrary, $\mathbf{C_{Sc2\text{-}nE\text{-}St}}$ adopting a bulky St monomer needs to overcome a much higher activation energy (14.8 kcal mol^{-1}, calculated by energetic span model[47]) via the transition state of $\mathbf{TS_{Sc2\text{-}nE\text{-}St}}$ to insert St, indicating that $\mathbf{Cat_{Sc2\text{-}nE}}$ is prone to polymerize E to give long PE units in this scenario. Therefore, to regulate the polymerization conditions, such as St concentration or PE pressure, the sequences and distribution can be finely adjusted. However, for the PE-ended mononuclear **Sc1** active species, $\mathbf{Cat_{Sc1\text{-}nE}}$ (Figure S6, red), the energy barrier for E insertion is 10.5 kcal mol^{-1} via the transition state of $\mathbf{TS_{Sc1\text{-}nE\text{-}E}}$, which is much higher than that for St insertion via the transition state of $\mathbf{TS_{Sc1\text{-}nE\text{-}St}}$ (2.4 kcal mol^{-1}). As a result, $\mathbf{Cat_{Sc1\text{-}nE}}$ quickly switches to St propagation and has difficulty forming a longer PE segment. Consequently, even in the copolymer with PE content of up to 50.9 mol % (Table 1, run 4), the melting peak arising from PE segments was not observed (**P1**).

For the binuclear catalyst, there is a third scenario, where the two Sc^{3+} are attached to a long PE chain and a long *s*PS chain,

https://doi.org/10.1021/acs.macromol.5c00169
Macromolecules 2025, 58, 2609−2618

$\mathbf{Cat}_{\mathbf{Sc2\text{-}nESt}}$ (Figure 7). The bulky St insertion to the active species Sc^{3+} attached to the *s*PS chain faces steric hindrance and needs to overcome a higher activation energy as compared to E insertion ($\mathbf{TS}_{\mathbf{Sc2\text{-}nESt\text{-}SS}}$, 18.9 kcal mol^{-1} vs $\mathbf{TS}_{\mathbf{Sc2\text{-}nESt\text{-}SE}}$, 10.3 kcal mol^{-1}, black line). On the contrary, St insertion to the active species Sc^{3+} attached to the PE chain via the transition state of $\mathbf{TS}_{\mathbf{Sc2\text{-}nESt\text{-}ES}}$ is a 7.5 kcal mol^{-1} energy advantage over E insertion, since the active metal center provides sufficient space for St coordination and the strong electron-donating phenyl ring stabilizes the generated intermediate $\mathbf{P}_{\mathbf{Sc2\text{-}nESt\text{-}ES}}$ (red line). These two contrasting insertion modes enable switching between *s*PS and PE segments, which is the origin of generating joint units in the copolymer main chain. These computational insights provide a reference for understanding the underlying mechanism responsible for forming long crystallizable PE and PS segments during the copolymerization catalyzed by the binuclear scandium catalyst, which is in agreement with experimental observations.

CONCLUSIONS

The syndioselective copolymerization of St and E using the novel binuclear scandium catalysts has been successfully achieved to afford copolymers with various styrene contents, which possess a unique multiblock structure composed of both long *s*PS and PE sequences and two T_m values. A copolymer with a styrene content of 72.0 mol % demonstrates exceptional mechanical properties, with up to 60.0 MPa tensile strength and an elongation at break of 7.7% as well as an impact resistance of 13.4 kJ m^{-2}, significantly surpassing those of commercial *s*PS. This is attributed to the toughening effect of the flexible long PE segments. A copolymer incorporating a St content lower than 20% exhibits an impact resistance exceeding 119 kJ m^{-2} better than that of PE, owing to the reinforcing effect of the rigid *s*PS segments. Microstructural characterization confirms that these copolymers show no significant phase separation between *s*PS and PE. This unique multiblock architecture synergistically combines the strength and rigidity of *s*PS with the ductility and toughness of PE, unveiling a probable approach to trade off the strength and toughness by regulating the chain structure and phase morphology. DFT calculations provide insights into the formation of continuous *s*PS and PE segments, which may only be achieved with the binuclear scandium catalyst having proper sterics and electronics to facilitate St or E propagation under certain homo *s*PS-ended or PE-ended active species.

ASSOCIATED CONTENT

Supporting Information

The Supporting Information is available free of charge at https://pubs.acs.org/doi/10.1021/acs.macromol.5c00169.

Detailed experimental procedures; St−E copolymerization data; steric map of scandium complexes; stress−strain curves for commercial HDPE; WAXD profiles of E−St copolymers; DFT calculations; GPC data; DSC data and NMR spectra of St−E copolymerization (PDF)

AUTHOR INFORMATION

Corresponding Authors

Shihui Li − *State Key Laboratory of Polymer Physics and Chemistry, Changchun Institute of Applied Chemistry, Chinese Academy of Sciences, Changchun 130022, China; School of Applied Chemistry and Engineering, University of Science and Technology of China, Hefei 230026, China;* orcid.org/0000-0002-4121-9119; Email: shihui-li@ciac.ac.cn

Dongmei Cui − *State Key Laboratory of Polymer Physics and Chemistry, Changchun Institute of Applied Chemistry, Chinese Academy of Sciences, Changchun 130022, China; School of Applied Chemistry and Engineering, University of Science and Technology of China, Hefei 230026, China;* orcid.org/0000-0001-8372-5987; Email: dmcui@ciac.ac.cn

Authors

Qiyuan Wang − *State Key Laboratory of Polymer Physics and Chemistry, Changchun Institute of Applied Chemistry, Chinese Academy of Sciences, Changchun 130022, China; School of Applied Chemistry and Engineering, University of Science and Technology of China, Hefei 230026, China*

Zhen Zhang − *State Key Laboratory of Polymer Physics and Chemistry, Changchun Institute of Applied Chemistry, Chinese Academy of Sciences, Changchun 130022, China; Shanxi Coal Chemical Industry Technology Research Institute, Xi'an 710000, China*

Yang Jiang − *State Key Laboratory of Polymer Physics and Chemistry, Changchun Institute of Applied Chemistry, Chinese Academy of Sciences, Changchun 130022, China; School of Applied Chemistry and Engineering, University of Science and Technology of China, Hefei 230026, China*

Complete contact information is available at: https://pubs.acs.org/10.1021/acs.macromol.5c00169

Author Contributions

The manuscript was written through contributions of all authors. All authors have given approval to the final version of the manuscript.

Funding

Natural Science Foundation of China.

Notes

The authors declare no competing financial interest.

ACKNOWLEDGMENTS

This work was partially supported by the NSFC (Project Nos. 22331010, U21A20279, 52073275, and U23B6011).

REFERENCES

(1) Tomotsu, N.; Ishihara, N.; Newman, T. H.; Malanga, M. T. Syndiospecific polymerization of styrene. *J. Mol. Catal. A:Chem.* **1998**, *128* (1), 167−190.

(2) Malanga, M. Syndiotactic Polystyrene Materials. *Adv. Mater.* **2000**, *12* (23), 1869−1872.

(3) Schellenberg, J.; Leder, H.-J. Syndiotactic polystyrene: Process and applications. *Adv. Polym. Technol.* **2006**, *25* (3), 141−151.

(4) Ishihara, N.; Seimiya, T.; Kuramoto, M.; Uoi, M. Crystalline syndiotactic polystyrene. *Macromolecules* **1986**, *19* (9), 2464−2465.

(5) Ishihara, N.; Kuramoto, M.; Uoi, M. Stereospecific polymerization of styrene giving the syndiotactic polymer. *Macromolecules* **1988**, *21* (12), 3356−3360.

(6) Schellenberg, J. Recent transition metal catalysts for syndiotactic polystyrene. *Prog. Polym. Sci.* **2009**, *34* (8), 688−718.

(7) Huang, J.; Liu, Z.; Cui, D.; Liu, X. Precisely Controlled Polymerization of Styrene and Conjugated Dienes by Group 3 Single-Site Catalysts. *ChemCatChem* **2018**, *10* (1), 42−61.

(8) Mahanthappa, M. K.; Waymouth, R. M. Titanium-Mediated Syndiospecific Styrene Polymerizations: Role of Oxidation State. *J. Am. Chem. Soc.* **2001**, *123* (48), 12093−12094.

(9) Nomura, K.; Komatsu, T.; Imanishi, Y. Syndiospecific Styrene Polymerization and Efficient Ethylene/Styrene Copolymerization Catalyzed by (Cyclopentadienyl)(aryloxy)titanium(IV) Complexes−MAO System. *Macromolecules* **2000**, *33* (22), 8122−8124.
(10) Nomura, K.; Liu, J. Half-titanocenes for precise olefin polymerisation: effects of ligand substituents and some mechanistic aspects. *Dalton Trans.* **2011**, *40* (30), 7666−7682.
(11) Galdi, N.; Buonerba, A.; Oliva, L. Olefin−Styrene Copolymers. *Polymers* **2016**, *8* (11), No. 405.
(12) Luo, Y.; Baldamus, J.; Hou, Z. Scandium Half-Metallocene-Catalyzed Syndiospecific Styrene Polymerization and Styrene−Ethylene Copolymerization: Unprecedented Incorporation of Syndiotactic Styrene−Styrene Sequences in Styrene−Ethylene Copolymers. *J. Am. Chem. Soc.* **2004**, *126* (43), 13910−13911.
(13) Rodrigues, A.-S.; Kirillov, E.; Lehmann, C. W.; Roisnel, T.; Vuillemin, B.; Razavi, A.; Carpentier, J.-F. Allyl ansa-Lanthanidocenes: Single-Component, Single-Site Catalysts for Controlled Syndiospecific Styrene and Styrene−Ethylene (Co)Polymerization. *Chem. - Eur. J.* **2007**, *13* (19), 5548−5565.
(14) Capacchione, C.; Proto, A.; Ebeling, H.; Mülhaupt, R.; Möller, K.; Spaniol, T. P.; Okuda, J. Ancillary Ligand Effect on Single-Site Styrene Polymerization: Isospecificity of Group 4 Metal Bis(phenolate) Catalysts. *J. Am. Chem. Soc.* **2003**, *125* (17), 4964−4965.
(15) Zambelli, A.; Oliva, L.; Pellecchia, C. Soluble catalysts for syndiotactic polymerization of styrene. *Macromolecules* **1989**, *22* (5), 2129−2130.
(16) Zinck, P.; Bonnet, F.; Mortreux, A.; Visseaux, M. Functionalization of syndiotactic polystyrene. *Prog. Polym. Sci.* **2009**, *34* (4), 369−392.
(17) Jaymand, M. Recent progress in the chemical modification of syndiotactic polystyrene. *Polym. Chem.* **2014**, *5* (8), 2663−2690.
(18) Laur, E.; Kirillov, E.; Carpentier, J. F. Engineering of Syndiotactic and Isotactic Polystyrene-Based Copolymers via Stereoselective Catalytic Polymerization. *Molecules* **2017**, *22* (4), No. 594.
(19) Aaltonen, P.; Seppala, J.; Matilainen, L.; Leskela, M. Polymerization of a styrene and ethylene mixture with a trichloro(2,6-di-tert-butylphenoxy)titanium/methylaluminoxane catalyst system. *Macromolecules* **1994**, *27* (12), 3136−3138.
(20) Mani, R.; Burns, C. M. Homo- and copolymerization of ethylene and styrene using titanium trichloride (AA)/methylaluminoxane. *Macromolecules* **1991**, *24* (19), 5476−5477.
(21) Soga, K.; Lee, D.-h.; Yanagihara, H. Copolymerization of ethylene with styrene using the catalyst system composed of Solvay-type $TiCl_3$ and $Cp_2Ti(CH_3)_2$. *Polym. Bull.* **1988**, *20* (3), 237−241.
(22) Longo, P.; Grassi, A.; Oliva, L. Copolymerization of styrene and ethylene in the presence of different syndiospecific catalysts. *Makromol. Chem.* **1990**, *191* (10), 2387−2396.
(23) Pellecchia, C.; Pappalardo, D.; D'Arc, M.; Zambelli, A. Alternating Ethylene−Styrene Copolymerization with a Methylaluminoxane-Free Half-Titanocene Catalyst. *Macromolecules* **1996**, *29* (4), 1158−1162.
(24) Oliva, L.; Mazza, S.; Longo, P. Copolymerization of ethylene and styrene with monocyclopentadienyltitanium trichloride/methylalumoxane catalyst. *Macromol. Chem. Phys.* **1996**, *197* (10), 3115−3122.
(25) Xu, G.; Lin, S. Titanocene−Methylaluminoxane Catalysts for Copolymerization of Styrene and Ethylene: Synthesis and Characterization of Styrene−Ethylene Copolymers. *Macromolecules* **1997**, *30* (4), 685−693.
(26) Nomura, K.; Okumura, H.; Komatsu, T.; Naga, N. Ethylene/Styrene Copolymerization by Various (Cyclopentadienyl)(aryloxy)-titanium(IV) Complexes−MAO Catalyst Systems. *Macromolecules* **2002**, *35* (14), 5388−5395.
(27) Zhang, H.; Nomura, K. Living Copolymerization of Ethylene with Styrene Catalyzed by (Cyclopentadienyl)(ketimide)titanium-(IV) Complex−MAO Catalyst System. *J. Am. Chem. Soc.* **2005**, *127* (26), 9364−9365.
(28) Arriola, D. J.; Bokota, M.; Campbell, R. E., Jr.; Klosin, J.; LaPointe, R. E.; Redwine, O. D.; Shankar, R. B.; Timmers, F. J.; Abboud, K. A. Penultimate Effect in Ethylene−Styrene Copolymerization and the Discovery of Highly Active Ethylene−Styrene Catalysts with Increased Styrene Reactivity. *J. Am. Chem. Soc.* **2007**, *129* (22), 7065−7076.
(29) Noh, S. K.; Lee, M.; Kum, D. H.; Kim, K.; Lyoo, W. S.; Lee, D.-H. Studies of ethylene−styrene copolymerization with dinuclear constrained geometry complexes with methyl substitution at the five-membered ring in indenyl of $[Ti(\eta^5{:}\eta^1\text{-}C_9H_5SiMe_2NCMe_3)]_2$ $[CH_2]_n$. *J. Polym. Sci., Part A:Polym. Chem.* **2004**, *42* (7), 1712−1723.
(30) Noh, S. K.; Yang, Y.; Won Seok, L. Investigation of ethylene and styrene copolymerization initiated with dinuclear constrained geometry catalysts holding polymethylene as a bridging ligand and indenyl as a cyclopentadienyl derivative. *J. Appl. Polym. Sci.* **2003**, *90* (9), 2469−2474.
(31) Guo, N.; Li, L.; Marks, T. J. Bimetallic Catalysis for Styrene Homopolymerization and Ethylene−Styrene Copolymerization. Exceptional Comonomer Selectivity and Insertion Regiochemistry. *J. Am. Chem. Soc.* **2004**, *126* (21), 6542−6543.
(32) Nomura, K.; Izawa, I.; Yi, J.; Nakatani, N.; Aoki, H.; Harakawa, H.; Ina, T.; Mitsudome, T.; Tomotsu, N.; Yamazoe, S. Solution XAS Analysis for Exploring Active Species in Syndiospecific Styrene Polymerization and 1-Hexene Polymerization Using Half-Titanocene−MAO Catalysts: Significant Changes in the Oxidation State in the Presence of Styrene. *Organometallics* **2019**, *38* (22), 4497−4507.
(33) Yi, J.; Nakatani, N.; Tomotsu, N.; Nomura, K.; Hada, M. Theoretical Studies of Reaction Mechanisms for Half-Titanocene-Catalyzed Styrene Polymerization, Ethylene Polymerization, and Styrene−Ethylene Copolymerization: Roles of the Neutral Ti(III) and the Cationic Ti(IV) Species. *Organometallics* **2021**, *40* (6), 643−653.
(34) Bueschges, U.; Chien, J. C. W. Metallocene−methylaluminoxane catalysts for olefin polymerizations. III. Reduction of η5-cyclopentadienyl trichlorides of titanium and zirconium. *J. Polym. Sci., Part A:Polym. Chem.* **1989**, *27* (5), 1525−1538.
(35) Grassi, A.; Zambelli, A.; Laschi, F. Reductive Decomposition of Cationic Half-Titanocene(IV) Complexes, Precursors of the Active Species in Syndiospecific Styrene Polymerization. *Organometallics* **1996**, *15* (2), 480−482.
(36) Yoon, S. W.; Kim, Y.; Kim, S. K.; Kim, S. Y.; Do, Y.; Park, S. Novel Dinuclear Half-Titanocene-Producing Styrene/Ethylene Copolymers Containing Syndiotactic Styrene/Styrene Sequences. *Macromol. Chem. Phys.* **2011**, *212* (8), 785−789.
(37) Li, X.; Wang, X.; Tong, X.; Zhang, H.; Chen, Y.; Liu, Y.; Liu, H.; Wang, X.; Nishiura, M.; He, H.; Lin, Z.; Zhang, S.; Hou, Z. Aluminum Effects in the Syndiospecific Copolymerization of Styrene with Ethylene by Cationic Fluorenyl Scandium Alkyl Catalysts. *Organometallics* **2013**, *32* (5), 1445−1458.
(38) You, F.; Xu, S.; Wang, J.; Zhai, J.; Wang, F.; Pan, L.; So, Y.-M.; Shi, X. Access to Derivatizable Octahydrofluorenyl Ligand: Half-Sandwich Rare-Earth Metal Complexes for Highly Syndiospecific (Co)Polymerization of Styrene. *Inorg. Chem.* **2022**, *61* (2), 1145−1151.
(39) Peng, D.-Q.; Yan, X.-W.; Zhang, S.-W.; Li, X.-F. Syndiotactic polymerization of styrene and copolymerization with ethylene catalyzed by chiral half-sandwich rare-earth metal dialkyl complexes. *Chin. J. Polym. Sci.* **2018**, *36* (2), 222−230.
(40) Liu, B.; Wang, L.; Wu, C.; Cui, D. Sequence-controlled ethylene/styrene copolymerization catalyzed by scandium complexes. *Polym. Chem.* **2019**, *10* (2), 235−243.
(41) Zhang, Z.; Kang, X.; Jiang, Y.; Cai, Z.; Li, S.; Cui, D. Access to Disentangled Ultrahigh Molecular Weight Polyethylene via a Binuclear Synergic Effect. *Angew. Chem., Int. Ed.* **2023**, *62* (4), No. e202215582.
(42) Zhang, Z.; Jiang, Y.; Lei, R.; Zhang, Y.; Li, S.; Cui, D. Proximity-Driven Synergic Copolymerization of Ethylene and Polar Monomers. *Macromolecules* **2023**, *56* (6), 2476−2483.
(43) Wu, C.; Liu, B.; Lin, F.; Wang, M.; Cui, D. cis-1,4-Selective Copolymerization of Ethylene and Butadiene: A Compromise

between Two Mechanisms. *Angew. Chem., Int. Ed.* **2017**, *56* (24), 6975−6979.
(44) Hay, J. N.; Wiles, M. The crystallization characteristics of ethylene block copolymers. *J. Polym. Sci., Polym. Chem. Ed.* **1979**, *17* (7), 2223−2231.
(45) Mirabella, F. M. Correlation of the melting behavior and copolymer composition distribution of Ziegler−Natta-catalyst and single-site-catalyst polyethylene copolymers. *J. Polym. Sci., Part B:Polym. Phys.* **2001**, *39* (22), 2800−2818.
(46) Zhang, M.; Wanke, S. E. Quantitative determination of short-chain branching content and distribution in commercial polyethylenes by thermally fractionated differential scanning calorimetry. *Polym. Eng. Sci.* **2003**, *43* (12), 1878−1888.
(47) Kozuch, S.; Shaik, S. How to Conceptualize Catalytic Cycles? The Energetic Span Model. *Acc. Chem. Res.* **2011**, *44* (2), 101−110.

https://doi.org/10.1021/acs.macromol.5c00169
Macromolecules 2025, 58, 2609−2618